

NAS Technical Report – NAS 05-004

Implementation of Finite Rate Chemistry Capability in OVERFLOW

M. E. Olsen *
NASA Ames Research Center
Moffett Field, CA 94035

D. K. Prabhu †
ELORET Corp.
Sunnyvale , CA 94087

T. Olsen ‡
ELORET Corp.
Sunnyvale , CA 94087

May 10, 2005

Abstract

An implementation of both finite rate and equilibrium chemistry have been completed for the OVERFLOW code, a chimera capable, complex geometry flow code widely used to predict transonic flowfields. The implementation builds on the computational efficiency and geometric generality of the solver.

Nomenclature

$\bar{\gamma}$	$\rho c^2/p$
χ	$\frac{\partial p}{\partial \rho} \Big _{\epsilon} - \frac{\rho}{\epsilon} \frac{\partial \rho}{\partial \epsilon} \Big _{p}$
ϵ	internal energy ($\int_0^T c_v dT$)
η	Self Similar Wall Distance for Wedge $((z-z_w)/\chi)$
ν_{rs}^b	Backward Stoichiometric Coefficient of species s in reaction r
ν_{rs}^f	Forward Stoichiometric Coefficient of species s in reaction r
∂_n	Spatial derivative in wall normal direction
ρ	total mass per unit volume ($\sum_s \rho_s$)
ρ_s	mass of species s per unit volume
c	Frozen Sound Speed, $\frac{\partial p}{\partial \rho} \Big _{s,c_i}$
c_s	Mass fraction of species s, ρ_s/ρ
h_T	stagnation enthalpy $(e_i + p/\rho + (u^2 + v^2 + w^2)/2)$
L	Wedge Length (χ/L)
u, v, w	Cartesian Velocity Components
x, y, z	Cartesian Position Coordinates

*Research Scientist, NASA Ames Research Center, Associate Fellow AIAA

†Senior Research Scientist, ELORET, Associate Fellow AIAA

‡Research Scientist, ELORET, Member AIAA

Introduction

Chemically reacting flows are of increasing importance to NASA's terrestrial and space missions. In cases where the flow geometry is complex, which includes most practical devices, ability to utilize overset grids greatly enhances NASA's ability to accurately model the flow physics. The OVERFLOW code is therefore an ideal platform for implementing chemical modeling capability. This provides the ability to predict performance and improve design of both reentry vehicles and propulsion systems. In this paper we discuss the approach for incorporating finite rate chemistry capability into OVERFLOW and present representative computations along with comparisons with experiment.

Method

The base code used is OVERFLOW[?] which is a finite difference, chimera(overset) grid capable, complex geometry flow code widely used for perfect gas prediction. Various ADI implicit treatments (Beam-Warming, Pulliam-Chausee diagonal, Symmetric LU Gauss Seidel) are available, along with a selection of spacial discretization options (central difference with scalar or matrix dissipation, Roe MUSCL upwinding, Yee's Symmetric TVD, etc.). Multigrid convergence acceleration is available, and improves the convergence of high Reynolds number viscous flows substantially.

Matrix dissipation combined with central space differencing and multigrid was shown to provide a rapid, robust solution method suitable for high speed, perfect gas flow with strong shock waves[?]. The first step in the generalization of the gas model of OVERFLOW was to implement the premixed chemical equilibrium gas model

of Liu and Vinokur[?]. Preliminary numerical experiments with this implementation verified that the central/matrix dissipation methodology continued to work with more general thermodynamics[?].

OVERFLOW was modified to replace the perfect gas model built into the code with a model assuming a gas made up of a mixture of thermally perfect ($p_i = \rho RT/\mathcal{M}_i$) gases. This modification affects a large fraction of the code, which used perfect gas assumptions to obtain pressure and temperature from the conservative field variables. Four extra field variables are added, corresponding to pressure, temperature, coefficient of thermal conductivity, and the new pressure derivative χ .

Chemically Reacting Reynolds Averaged Navier Stokes Equations

The Reynolds averaged Navier-Stokes equations, written in conservation law form are

$$\frac{\partial Q}{\partial t} + \frac{\partial F}{\partial x} + \frac{\partial G}{\partial y} + \frac{\partial H}{\partial z} = 0 \quad (1)$$

Where

$$Q = [\rho, \rho u, \rho v, \rho w, \rho \epsilon,] \quad (2)$$

$$F = \left[\rho u, \rho u^2 + p + \tau_{xx}, \rho uv + \tau_{xy}, \rho uw + \tau_{xz}, \rho u(\epsilon_T + p + \tau_{xx}) + v\tau_{xy} + w\tau_{xz} + k \frac{\partial T}{\partial x} \right] \quad (3)$$

$$G = \left[\rho v, \rho v u + \tau_{yx}, \rho v^2 + p + \tau_{yy}, \rho vw + \tau_{yz}, \rho v(\epsilon_T + p + \tau_{yy}) + w\tau_{yz} + u\tau_{yx} + k \frac{\partial T}{\partial y} \right] \quad (4)$$

$$H = \left[\rho w, \rho w u + \tau_{zx}, \rho w v + \tau_{zy}, \rho w^2 + p + \tau_{zz}, \rho w(\epsilon_T + p + \tau_{zz}) + u\tau_{zx} + v\tau_{zy} + k \frac{\partial T}{\partial z} \right] \quad (5)$$

The Navier-Stokes equations for a chemically reacting gas are similar to this set, except that the 1st equation (mass conservation) is replaced by n_s equations, one for each chemical species.

$$\partial_t \rho_i + \partial_x (u \rho_i + (D \partial_x \rho_i)) + \partial_y (v \rho_i + (D \partial_y \rho_i)) + \partial_z (w \rho_i + (D \partial_z \rho_i)) = \dot{w}_i \quad (6)$$

These equations add a mass diffusion term ($\partial_\xi D (\partial_\xi \rho_i)$) and a source term \dot{w}_i . The standard form for the source

terms is

$$\dot{w}_i = \sum_r^{nr} \mathcal{M}_s \left(\nu_{ri}^f - \nu_{ri}^b \right) k_r^f A_{rs} \quad (7)$$

$$A_{rs} = \prod_s^{ns} \left(\frac{\rho_s}{\mathcal{M}_s} \right)^{\nu_{rs}^f} - \frac{(p/p_{ref})^{-\Delta \nu_r}}{K_r^e} \prod_s^{ns} \left(\frac{\rho_s}{\mathcal{M}_s} \right)^{\nu_{rs}^b} \quad (8)$$

where the r sums the contributions of the individual reactions, k^f is the forward reaction rate and K_r^e is the equilibrium constant (a pure function of temperature), p_{ref} is the pressure reference for K^e , and $\Delta \nu_r = \sum_s^{ns} \nu_{rs}^f - \sum_s^{ns} \nu_{rs}^b$.

In this form, the significance of K_r^e is obvious. In the case where the mass fractions satisfy the relation

$$\left(\frac{p}{p_{ref}} \right)^{\Delta \nu_r} K_r^e \prod_s^{ns} \left(\frac{\rho_s}{\mathcal{M}_s} \right)^{\nu_{rs}^f} = \prod_s^{ns} \left(\frac{\rho_s}{\mathcal{M}_s} \right)^{\nu_{rs}^b} \quad (9)$$

for reaction r , the source term for this particular reaction will be zero. K_r^e can be calculated from equilibrium thermodynamics, or can be specified independently. Both options are available in the current implementation.

The current implementation is a loosely coupled formulation. The original Navier-Stokes equations (1-5) (with additional terms corresponding to transport of mass and energy via species diffusion) are solved, holding the species fractions constant. The species equations (6) are then solved holding the velocities and temperatures from the mean flow equations just calculated. This over-specifies the problem, as the mass conservation equation is contained in the species mass conservation equations. Although various methods of removing this over-specification were attempted, the current method simply ignores the over-specification, and utilizes the ρ_i to get the partial pressures, and ρ as the total mass density. As the solution converges, the ratio $\sum_i^{ns} \rho_i / \rho$ is used to verify convergence along with the equation residual levels.

Generalization of the Thermodynamic Model

At the start of each step, just before the viscosity is calculated, the temperature is found for each point from the current internal energy and species concentrations, via a Newton-Raphson iteration. This temperature can then be used to find the pressure at each point, by summing the partial pressures of each gas ($p = \sum_{species} p_{species}$). The Prandtl number is calculated from Eucken's relation[?]. The gas constant is calculated from the species fractions and their molecular weights.

The internal energy and absolute entropy of each species as a function of temperature are input as a table to generalize the thermodynamic model. The table has the following format:

$$\begin{array}{l}
 \text{species } 1 \\
 \vdots \\
 \text{species } N_t
 \end{array}
 \begin{array}{l}
 \left(\begin{array}{l}
 N_T \quad T_0 \quad \Delta T \\
 \mathcal{N} \mathcal{A} \mathcal{M} \mathcal{E}_1 \\
 \mathcal{M}_1 \quad \Delta H_{f1} \\
 T_0 \quad \hat{\epsilon}_0/\mathcal{R} T \quad \hat{s}_0/\mathcal{R} \\
 T_1 \quad \hat{\epsilon}_1/\mathcal{R} T \quad \hat{s}_1/\mathcal{R} \\
 \dots \\
 T_{N_T} \quad \hat{\epsilon}_{N_T}/\mathcal{R} T \quad \hat{s}_{N_T}/\mathcal{R}
 \end{array} \right) \\
 \vdots \\
 \left(\begin{array}{l}
 \mathcal{N} \mathcal{A} \mathcal{M} \mathcal{E}_{N_s} \\
 \mathcal{M}_{N_s} \quad \Delta H_{fN_s} \\
 T_0 \quad \hat{\epsilon}_0/\mathcal{R} T \quad \hat{s}_0/\mathcal{R} \\
 T_1 \quad \hat{\epsilon}_1/\mathcal{R} T \quad \hat{s}_1/\mathcal{R} \\
 \dots \\
 T_{N_T} \quad \hat{\epsilon}_{N_T}/\mathcal{R} T \quad \hat{s}_{N_T}/\mathcal{R}
 \end{array} \right)
 \end{array}$$

The first line gives the number of (equi-spaced) temperature values used (N_T), the starting temperature ($T_0(K^\circ)$), and the temperature spacing ($\Delta T(K^\circ)$). The second line is chemical formula for the species, such as H₂O for water, O₂ for diatomic oxygen, etc. The next line is the molecular weight in kg/kmole and the heat of formation in KJoules/kg. The next N_T lines are the values of $T(K^\circ)$, internal energy (non-dimensionalized by $\mathcal{R}(T)$), and entropy (non-dimensionalized by \mathcal{R}). This is then followed by a similar set of lines for each species in turn. The order of the species in this file is the order of the species stored in the solution file, and the order of species for specifying reaction rates, etc.

This choice of functional form for the table, and hence the cubic spline fits also results in a smaller variation over in the functional values (at least for ϵ) over large temperature ranges. A species with constant specific heat would have the $\epsilon/\mathcal{R}T$ column a constant. Tables have been created for 5 species air ([N₂, O₂, NO, N, O], from [?]), and hydrogen-air ([H₂, N₂, O₂, HO, H, O, H₂O, HO₂, H₂O₂], from NIST(<http://webbook.nist.gov/chemistry/>) polynomial fits).

Polynomial fits, such as the Lewis, or NIST curve fits may be input by creating a table by evaluating the polynomials and writing out the values of T , $\hat{\epsilon}/(\hat{\mathcal{R}}T)$ and $\hat{s}/\hat{\mathcal{R}}$. Energy and absolute entropy are both input, so that chemical equilibrium or finite rate chemistry may be calculated. This also allows the backward rate for the

chemistry to be calculated from the forward rate and the second law of thermodynamics.

The field equations for convection of species are also available in the perfect gas version of OVERFLOW. These were replaced with a generalized upwind or central convection, mass diffusion, and generalized chemical source module. These are currently solved uncoupled from the fluid and turbulence field equations. A fast source calculation procedure was implemented, so that the source flux and Jacobian requires about the same amount of computational effort as the efficient Pulliam-Chausee diagonal fluids step.

Chemical Reaction Specification

The chemical reactions are input in the OVERFLOW input file, in a new namelist section in the input file \$CHEM. The elements of this namelist are:

NREACT	number of reactions
NELEM	number of elements
SCOEF(ISPECIES,JELEM)	elements atoms in species
VNUF(IREACT,ISPECIES)	stoichiometric coefficients
VNUB(IREACT,ISPECIES)	
FCOEF(:,IREACT)	reaction rates
ECOEF(:,IREACT)	

are all specified in this section. William Chan has written a version of OVERGRID[?] which facilitates the input of these variables. This software, reads the thermodynamics input files *gas.tbl* described above, parses out the SCOEF matrix from the species names, and then allows reactions to be specified in an intuitive manner. The system also checks for element balance among the chemical reactions input, and requires the reactions to balance elements between forward and backward sides.

A decision was made to consistently use SI units(kmoles, m, kg, K^o and sec) when dimensional values were necessary, such as for T_∞ , p_∞ , reaction rates, etc. A great deal of the chemical reaction data is in cgs (moles, cm, g, and sec) units and factor of 10^{-3} will transform a reaction rate from $\text{cm}^3/(\text{mole sec})$ to $\text{m}^3/(\text{kmole sec})$. The forward rate is input in the Arrhenius form $k_f = C_1(T)^{C_2} \exp(C_3/T)$, and the backward rate is determined either from an equilibrium coefficient $K_r^e = k_b/k_f = K^e(\text{ecoeff}_r, T)$ in the modified Arrhenius form used in reference[?], or directly from the 2nd law of thermodynamics.

The reactions are specified separately, so that each third body reaction is input separately. This greatly expands the size of this input section, but allows for complete generality in fixing the forward and backward

rate of each reaction for the various third bodies. The chemical source calculation procedure goes through the complete reaction set, and groups reactions from the same third body reaction together, accounting for the variations in the forward and backward rates among the group of various third body species, for computational efficiency.

For the species equations, both central and 2nd order upwind are available, and solutions using both approaches are given in the results section. There are cases for which the upwind method is more robust, but once initial transients are eliminated, the central space version is more robust and accurate.

Transport Properties

The diffusion operator for the species equations is 2nd order accurate, and the binary diffusion coefficients and laminar viscosities are given by Leonard-Jones theory, with a Wilke mixing rule. Eucken's relation is used to give the molecular thermal conductivity, or Prandtl number, of the gas mixture. Turbulence is modeled by any of the available turbulence models in OVERFLOW. The effect of turbulence is only to increase the effective viscosity, binary diffusivity, and heat transfer. No enhancement of the reaction rates is currently modeled.

Non-Premixed Chemical Equilibrium Capability

Along with the new finite rate capability, an ability to accurately simulate flows in chemical equilibrium has been implemented. This capability was envisioned as a means of providing a robust starting solution capability for difficult flowfields. This capability does not require that the flow be premixed, so that equilibrium diffusion flame calculations are possible. For flowfields where chemical equilibrium is a valid assumption, this provides a robust and more simply specified simulation capability.

This capability is provided by a similarity transformation of the species variables. The species can be thought of as composed of linear combinations of the elements. For instance, water (H_2O) can be thought of as 2 parts hydrogen to one part oxygen (on a molar basis). A linear combination of the species then can be used to compute the molar concentration of each element, given the species concentrations. For a chemical system composed of n_e elements and n_s species, there are n_e linear equations which will give the amount of each element given the species concentrations. Furthermore, on

physical grounds, these n_e equations are independent, and thus define an n_e -dimensional subspace within the n_s dimensional species space. A method equivalent to Gram-Schmidt orthogonalization can then generate the remaining $n_s - n_e$ linear relations which will transform the original species variables into a new set of variables, where n_e of the new variables correspond to the elements, and the remaining $n_s - n_e$ variables correspond to the degrees of reaction freedom of the system chemical system.

This transformation can be (and has been) automated, and has some desirable properties which merit exploration. One of these properties is that transforming the species equations to this new independent variable set separates out the n_e zero eigenvalues of the source Jacobian matrix. More than this, these variables have zero source, so they could be separated from the other $n_s - n_e$ variables, and solved as simple convection diffusion equations. The other 'reaction freedom' variables can then be solved as the original species set, with non-zero sources, and a matrix block size reduced by the n_e elements separated out at considerable computational savings.

Currently, this "element splitting" is utilized to implement the non-premixed chemical equilibrium capability of the code. The species are split, and the equations for the element conservation are solved. The 'reaction freedom' variables are solved for by enforcing chemical equilibrium at each point.

Multigrid, Relaxation, and Chemistry-Fluid Coupling

The multigrid method[?] has been modified to enhance the robustness of the method. The original multigrid method used a linear interpolation of the conservative variables to map the coarse grid solution onto the next finer grid. This interpolation was replaced with a linear interpolation of the variables $[\rho, u, v, w, \epsilon]$, which ensures a positive value of ϵ on the finer grid if ϵ is positive on the coarser grid. With this modification, the multigrid method continues to be a net win, enhancing robustness and improving convergence rates.

The Pulliam-Chaussee diagonal algorithm is used for the mass, momentum and energy equations, and enhances the computational efficiency. This implicit operator requires that the eigensystem be modeled correctly. The frozen sound speed $\left. \frac{\partial p}{\partial \rho} \right|_{s, c_i}$, is calculated by $(\bar{\gamma} p / \rho)$, with $\bar{\gamma} = 1 + \frac{R}{C_v}$.

The chemistry implementation is currently a loosely

coupled approach, with the changes in mass, momentum and energy variables $\{\rho, \rho u, \rho v, \rho w, \rho e\}$ solved for holding species concentration fixed, and then changes in species concentration $\{c_i\}$ are determined by solving the conservative form of the species transport equations holding the conservative variables constant.

Boundary Conditions

A new boundary condition was implemented for chemically reacting flowfields, the catalytic fixed temperature wall. The non-catalytic boundary condition for the species is zero gradient in species fractions. A catalytic wall boundary condition is given as

$$\begin{aligned} \mathcal{D}\partial_n(\rho_{N_2}) &= \rho_N \gamma_c \left(\frac{\mathcal{R}T}{2\pi\mathcal{M}_N} \right)^{\frac{1}{2}} \\ \mathcal{D}\partial_n(\rho_N) &= -\rho_N \gamma_c \left(\frac{\mathcal{R}T}{2\pi\mathcal{M}_N} \right)^{\frac{1}{2}} \\ \mathcal{D}\partial_n(\rho_{O_2}) &= \rho_O \gamma_c \left(\frac{\mathcal{R}T}{2\pi\mathcal{M}_O} \right)^{\frac{1}{2}} \\ \mathcal{D}\partial_n(\rho_O) &= -\rho_O \gamma_c \left(\frac{\mathcal{R}T}{2\pi\mathcal{M}_O} \right)^{\frac{1}{2}} \\ \mathcal{D}\partial_n(\rho_{NO}) &= 0 \end{aligned} \quad (10)$$

where the value of γ_c is 0 for a non-catalytic wall, or 1 for a fully catalytic wall, and \mathcal{D} is the binary diffusion coefficient.

This is implemented in a general way by defining the diffusion potential of the species j as

$$\mathcal{W}_j = \rho_j \left(\frac{\mathcal{R}T}{2\pi\mathcal{M}_j} \right)^{\frac{1}{2}}$$

then we can write a general version of this boundary condition as

$$\mathcal{D}\partial_n(\rho_j) = \sum_k C_{jk} \mathcal{W}_k \quad (11)$$

where C_{jk} is a $n_s \times n_s$ matrix.

Results

Inviscid Wedge Flow

This flowfield is a self similar flowfield useful for gauging the ability to capture shocks at oblique angles to the grid, and to obtain the external inviscid flowfield downstream of the shock. The case considered here is a 30° wedge, at $M=25.083$, with freestream static conditions of $p_\infty = 100\text{KPa}$, $T_\infty = 298^\circ\text{K}$. The species for this case

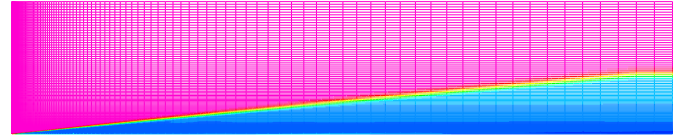


Figure 1: $30^\circ M=25$ Inviscid Wedge Grid, Colored by Axial Velocity. (Flow is inclined 30° to horizontal in this figure)

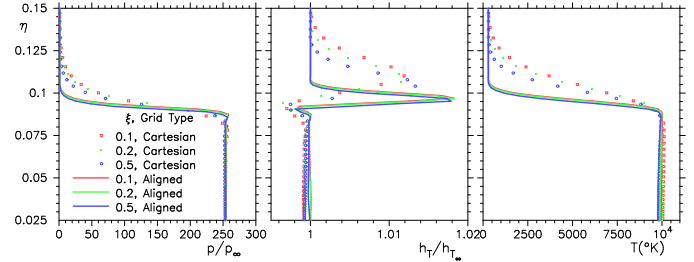


Figure 2: Inviscid $M=25$ Wedge, Profiles of Pressure, Total Enthalpy, Temperature and γ

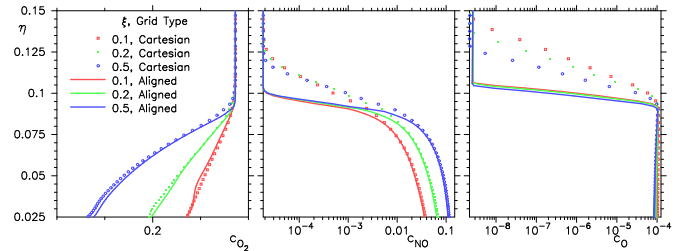


Figure 3: Inviscid $M=25$ Wedge, Mass Fraction Profiles (Same Legend as Figure 2).

are $\{N_2, O_2, NO, N, O\}$. The thermodynamic data for these species ($cv(T)$) are from the calculations outlined in Liu[?].

This flowfield was computed on two different grid systems. The first was a ‘‘shock aligned’’ grid system, with grid lines at constant angle from the origin. As this is a self-similar flowfield, the shock runs down the grid lines and the grid alignment is as advantageous as can be hoped for in a practical problem. The second grid system is simply a Cartesian box grid, where the shock crosses the grid lines as it moves down the wedge.

A converged solution on the Cartesian grid is shown in Figure 1. The capture of the oblique shock is clearly demonstrated, with uniform conditions obtained on both sides of the shock. The shock crosses the grid system obliquely, with the shock moving out approximately one grid line for every grid line moved downstream.

Profiles of pressure, total enthalpy and temperature are shown in Figure 2. The pressure profile shows minimal overshoot, with good similarity between the various axial locations for the shock aligned grid. The non-aligned grid has appreciably more smeared shocks, but recovers the post shock conditions well, including total enthalpy. The total enthalpy is well conserved (for this flowfield it is constant), with errors, even at the shock, less than 2%. Total enthalpy errors behind the shock are less than 0.1%. The post shock temperature reached in this flowfield is $10,000^\circ\text{K}$.

The species mass fractions are shown in Figure 3. A great deal of the diatomic oxygen (O_2) is dissociated across the shock, and is transformed into nitrous oxide (NO). Elemental oxygen (O) and nitrogen (N) are at low levels post shock.

The matrix dissipation and ADI scheme handle this condition well regardless of the relative alignment of the shock and grid. The only difference between the solutions are some artifacts of the details of the solution near the nose of the wedge which are faithfully carried downstream, but the shock position and post shock solution are independent of the grid alignment for this case, which features a shock sufficiently large to produce dissociated flow. The ability to produce good solutions without excessive attention to shock aligning the grid is an important characteristic of this solution methodology.

2D Circular Blunt Body Flow

As a comparison to other codes, a solution for a 1m and 0.01m radius circular blunt body at 40km altitude, $u_\infty = 4$ km/sec (Figure 4) is compared with solutions from GASP. The flow conditions for this case are $M_\infty = 12.7$, $Re_r = 9690$, $T_\infty = 251.05^\circ\text{K}$, and $p_\infty = 277.5\text{Pa}$. The freestream mass fractions are $c_{\text{N}_2} = 0.767$, $c_{\text{O}_2} = 0.233$ with traces of NO , N , and O . The wall boundary conditions is a fully catalytic fixed temperature, with $T_w = 2553^\circ\text{K}$. The two radii give solutions with Reynolds numbers which differ by a factor of 100.

The dimensions of the finest grid were 101×101 , and the solution was evaluated on coarser grids of 51×51 and 26×26 to assess grid convergence. The coarser grids were obtained from the finer grid by successively deleting every other point. Wall normal spacing for the finest grids was 3×10^{-5} for both GASP and OVERFLOW. The solutions were verified to be grid converged, by comparison with coarser grids.

Profiles of the thermodynamic variables along the

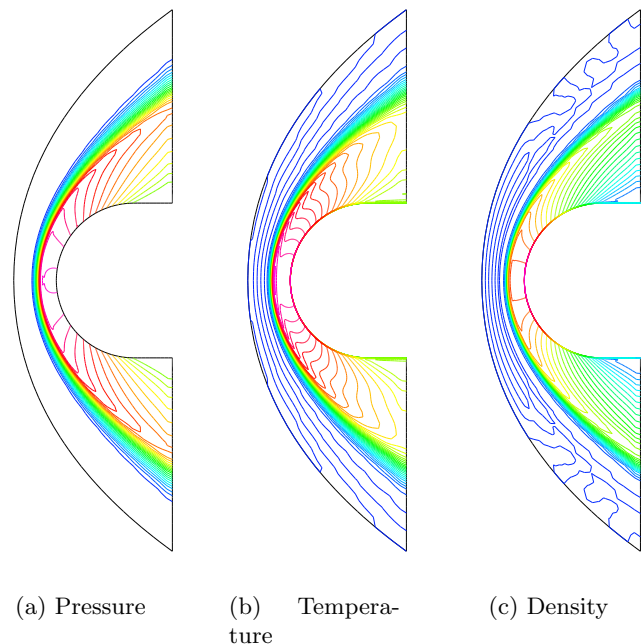


Figure 4: Circular Cylinder Flowfield: $M_\infty = 12.7$, $r = 1\text{m}$, $h = 40\text{km}$, $|v| = 4.04\text{km/s}$

stagnation streamline are shown in Figure 6. Total enthalpy is well conserved across the shock, and the predictions of GASP and the two reaction models are in good agreement. Pressure is also in very good agreement, and the OVERFLOW solution appears to be grid resolved on the 51×51 grid. Temperature and density are not in as good agreement as the other variables, however.

A possible reason for this can be seen from Figure 5, where the stagnation line species concentrations are shown. The levels of monatomic nitrogen and oxygen are well predicted, but there is a slight disagreement in the predictions for NO , N_2 , and O_2 . These differences are consistent with differences in the K_r^e representations, as the results can be brought into much closer agreement by altering the reference pressure for K_r^e . As there is some uncertainty in the various estimates of K_r^e for these reactions, this agreement is probably as good as can be expected.

Skin friction predictions agree well with GASP (Figure 7), with some slight differences between the two codes and the two transports models.

F4 Nozzle Flow

Another important test case for chemically reacting flows are nozzle flowfields. Test 10-97 (figure 8) of the HHSFD database is the flow in the ONERA F4 wind

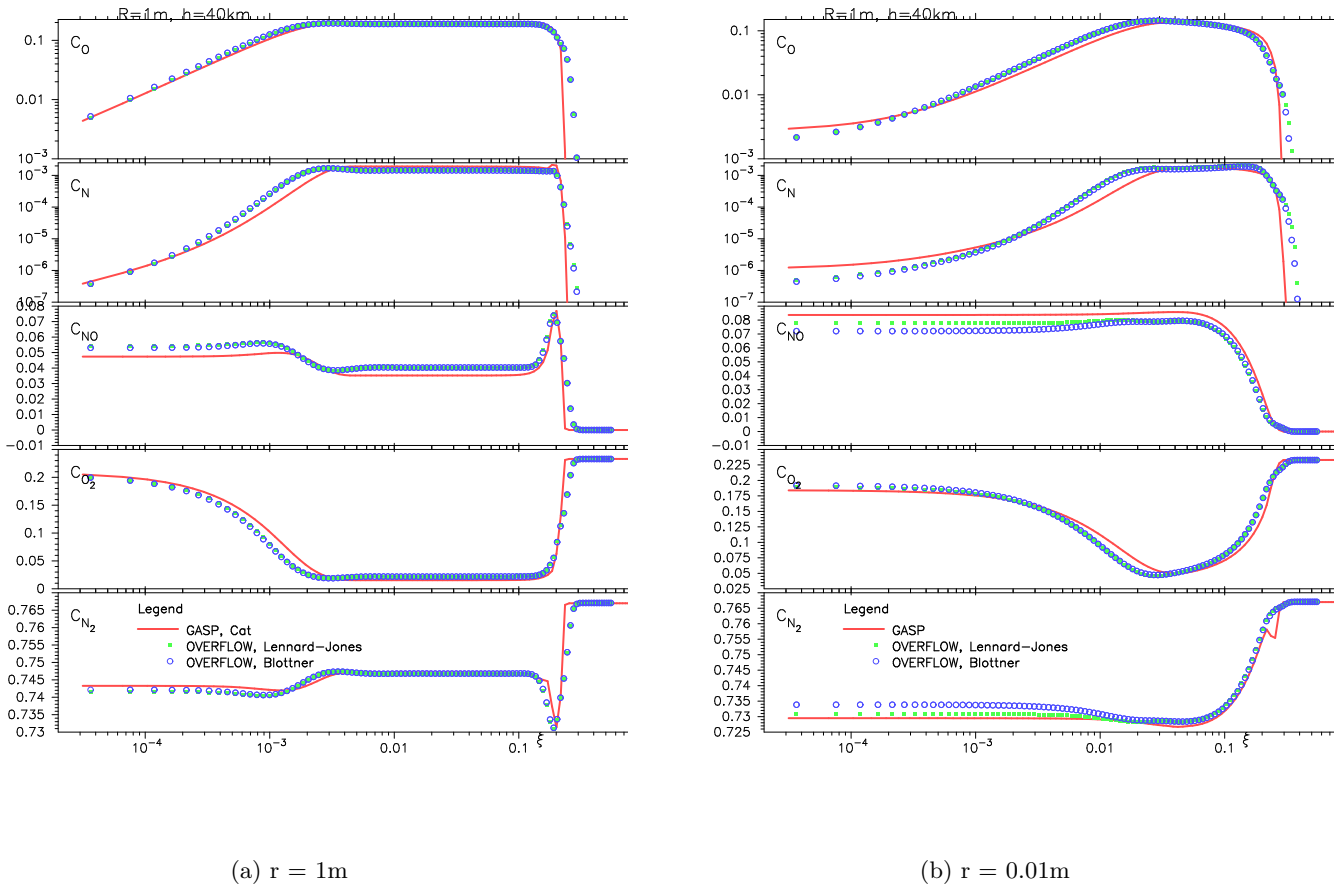


Figure 5: 2D Cylinder Stagnation Line Mass Concentrations, $M_\infty = 12.7$, $h = 40\text{km}$, $|v| = 4.04\text{km/s}$

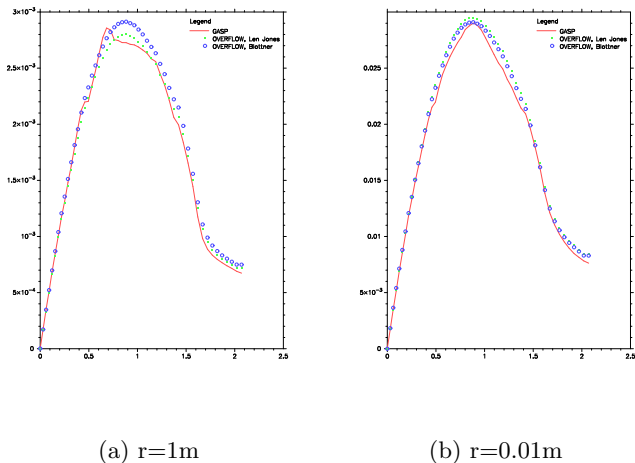


Figure 7: Circular Cylinder Skin Friction: $M_\infty = 12.7$, $h = 40\text{km}$, $|v| = 4.04\text{km/s}$



Figure 8: T10-97 Pressure Predictions, Finite Rate

tunnel nozzle. This flowfield utilizes synthetic air, containing only nitrogen and oxygen (no argon, CO_2 , etc.), with mass fractions of 7/9 and 2/9 respectively. The stagnation chamber of the flowfield has extremely high enthalpy (100 times standard sea level conditions) and extremely high pressure (37.3 MPa). The flow then expands out a axisymmetric nozzle to near vacuum conditions ($p = 52\text{Pa}$). The flowfield has been computed with a variety of codes[?], providing a useful comparison with other codes, as well as experimental data.

Inlet conditions are highly dissociated subsonic flow. Plug flow in chemical equilibrium was imposed at the inlet face of the flowfield, and p_t and T_t were chosen to produce the correct enthalpy and pressure in the stagnation

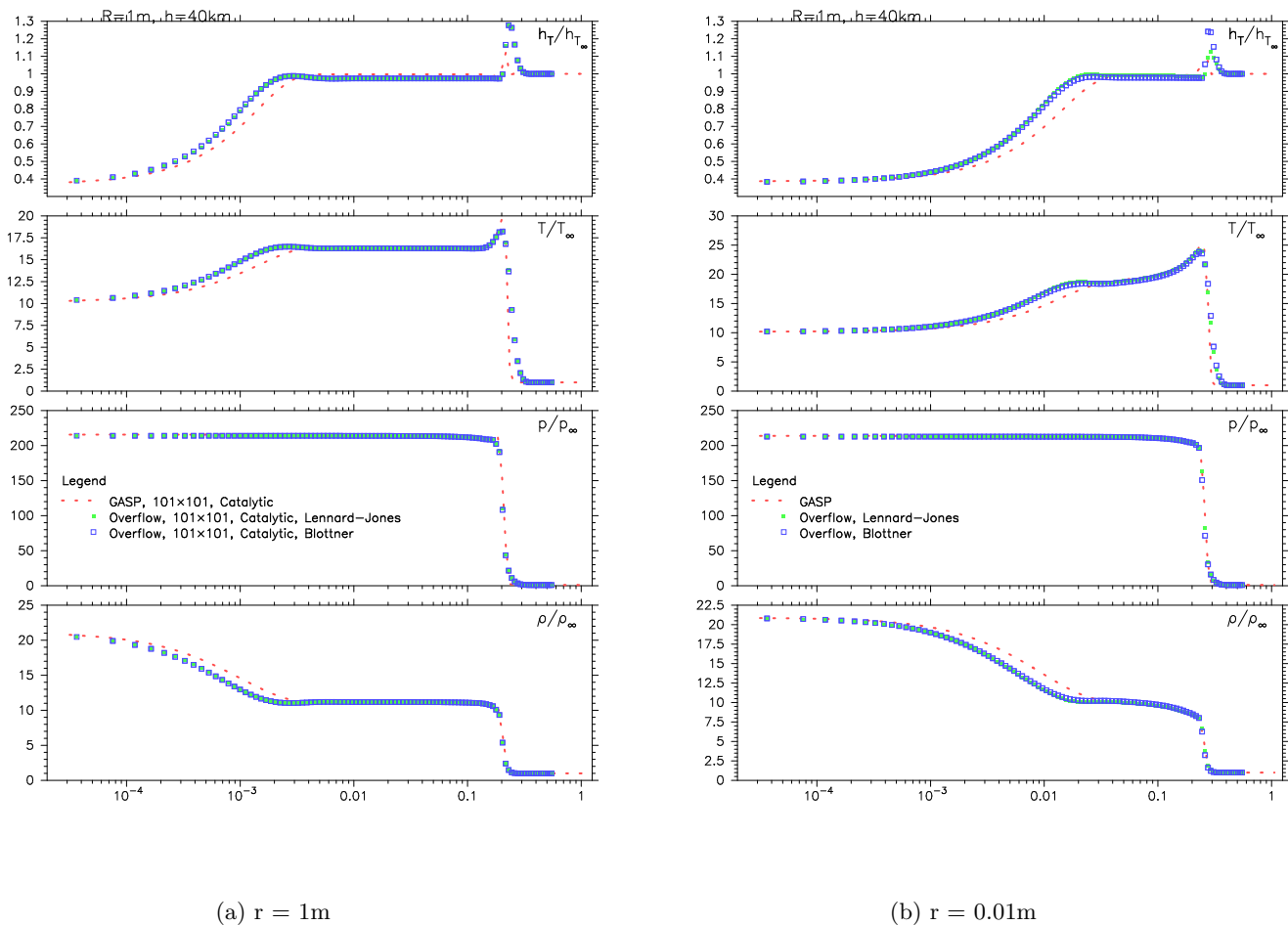


Figure 6: 2D Cylinder Stagnation Line Thermodynamic State, $M_\infty = 12.7$, $h = 40\text{km}$, $|\mathbf{v}| = 4.04\text{km/s}$

tion chamber. The Spalart-Allmaras turbulence model was used, and the initial ν_T was set to 0.1 laminar viscosity. Tunnel walls are modeled as constant temperature no-slip boundaries, and the exit plane boundary condition is simple extrapolation.

The flow is close to being in chemical equilibrium, and equilibrium codes are as successful as finite rate codes in predicting the nozzle wall pressures. Figure 9 shows a comparison of the wall pressure predictions of the code with experimental values. Also shown are the wall pressure predictions of the code in equilibrium mode (using the Parks equil. coefficients), and the premixed chemical equilibrium version of OVERFLOW [?].

Exit pressures are reasonably well predicted for this case, as shown in figure 10, and are very much in line with predictions of other nonequilibrium codes for this case. The exit temperature is also well in line with other predictions, and agrees well within the experimental uncertainty (figure 11). A final check is provided by the NO

mass fraction prediction, as seen in figure 12. This prediction agrees well with other predictions for this quantity, in terms of the the exit level, and how quickly it approaches this value.

1 Conclusions

Finite rate and equilibrium chemistry capability has been added to a version of the OVERFLOW code. The implementation is capable of predicting both propulsion and reentry flowfields, and extends the overset capability of OVERFLOW into reacting flowfields. Matrix dissipation is proving to be a capable methodology for predicting flowfields with strong shocks and large expansions.

Acknowledgments

The first author wishes to acknowledge the benefit of discussions and help of Dr. Sankaran Venkateswaran, Dr Yen Liu, and Dr. Marcel Vinokur in implementing finite

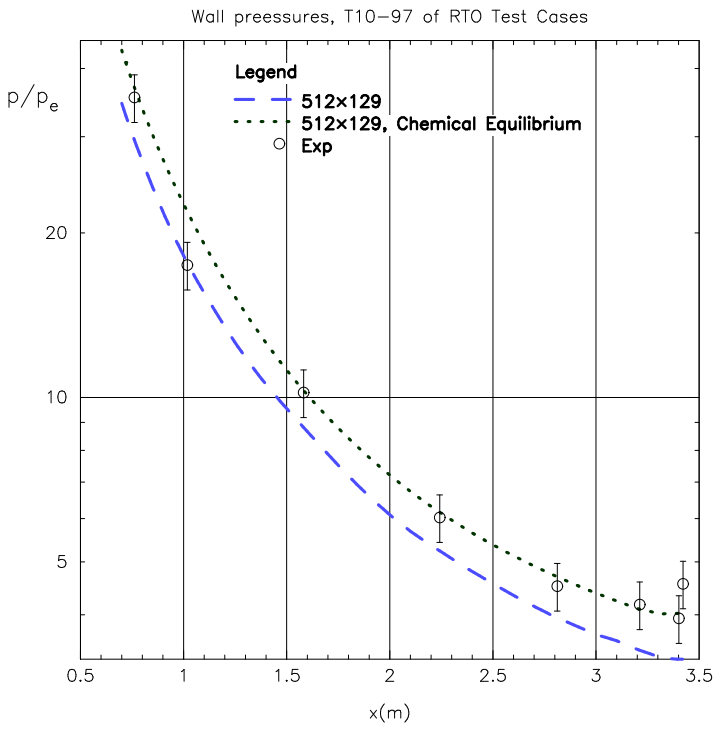


Figure 9: Wall Pressure Field Predictions, Comparison with Experiment

rate chemistry in OVERFLOW. Their unfailing assistance and knowledge of reacting flow simulations were of great help throughout this process.

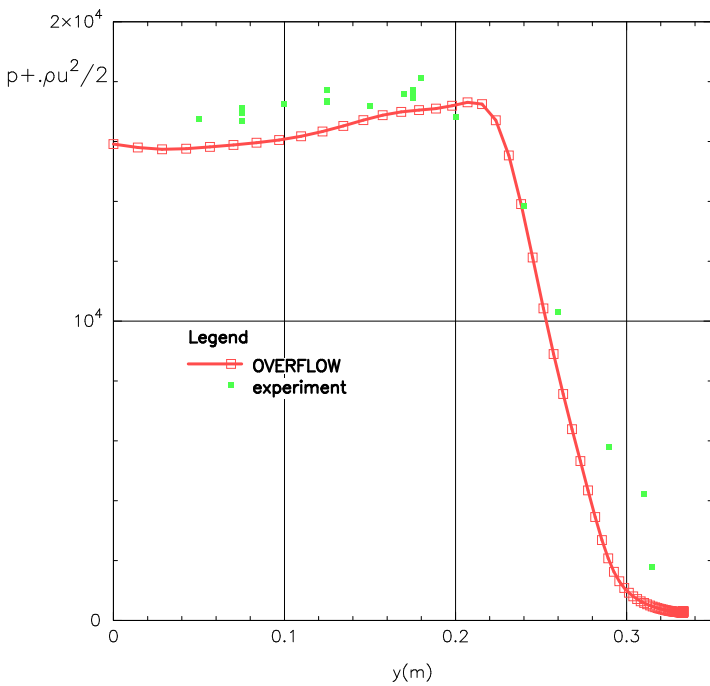


Figure 10: Exit Plane Pitot Pressure Field Predictions, Comparison with Experiment

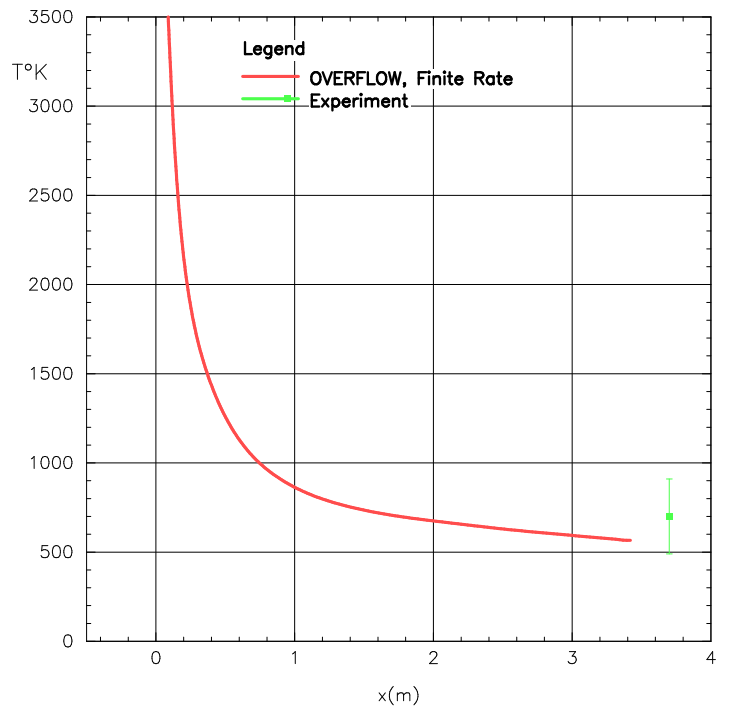


Figure 11: Centerline Temperature Predictions

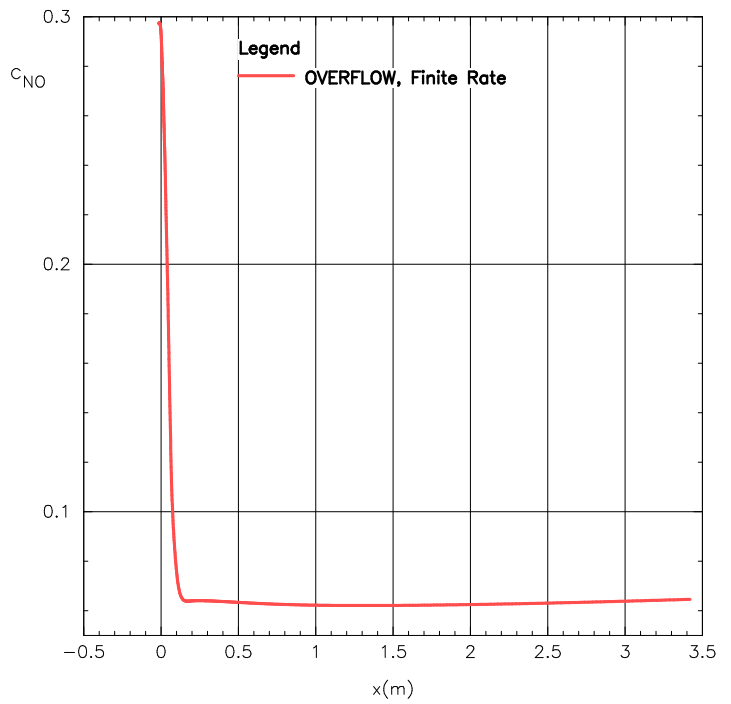


Figure 12: Centerline NO Mass Fraction Predictions

References

- [1] Buning, Pieter G. et al. Overflow user’s manual. Version 1.8, NASA Ames Research Center, February 1998.
- [2] Olsen, Michael E. and Dinesh K. Prabhu. “Appli-

- cation of OVERFLOW to Hypersonic Perfect Gas Flowfields”. AIAA Paper 2001-2664, 2001.
- [3] Liu, Yen and Vinokur, Marcel. “Equilibrium Gas Flow Computations. I. Accurate and Efficient Calculation of Equilibrium Gas Properties”. AIAA Paper 89-1736, 1989.
- [4] Olsen, M. , Liu, Y., Vinokur, M., and Olsen, T. “Implementation of Premixed Equilibrium Chemistry Capability in OVERFLOW”. AIAA Paper 2003-0962, 2003.
- [5] Rosner, Daniel E. . “*Transport Processes in Chemically Reacting Flow Systems*”. Dover Publications, 2000.
- [6] Chan, William M. “The OVERGRID Interface for Computational Simulations on Overset Grids”. AIAA Paper 2002-3188, June 2002.
- [7] Park, Chul . “*Nonequilibrium Hypersonic Aerothermodynamics*”. John Wiley and Sons, 1990.
- [8] Jespersen, D, Pulliam, T. H., and P.G. Buning. Recent enhancements to overflow. AIAA Paper 97-0664, January 1997.
- [9] Sagnier, P. and Muylaert, M. “Synthesis of the Contributions to the Test Case T10-97 Wind Tunnel Nozzle”. First Europe-US High Speed Flow Database Workshop-Part 2, November 12-14 2000, Naples, Italy, 1997.